A run in the wind: favorable winds make the difference in drone delivery

Conference Paper · July 2021

DOI: 10.1109/DCOSS52077.2021.00031

3 authors:

Lorenzo Palazzetti
University of Florence
19 PUBLICATIONS **99** CITATIONS
SEE PROFILE

Cristina M. Pinotti
Università degli Studi di Perugia
214 PUBLICATIONS **1,901** CITATIONS
SEE PROFILE

Giulio Rigoni
Sapienza University of Rome
12 PUBLICATIONS **86** CITATIONS
SEE PROFILE

A run in the wind: favorable winds make the difference in drone delivery

Lorenzo Palazzetti
University of Florence & University of Perugia, Italy
lorenzo.palazzetti@unifi.it

Cristina M. Pinotti
Dept. of Math. and Comp. Sc. University of Perugia, Italy
cristina.pinotti@unipg.it

Giulio Rigoni
University of Florence & University of Perugia, Italy
giulio.rigoni@unifi.it

***Abstract*—The impact on the energy consumption of flying drones in favorable winds is investigated in this paper. A tandem system is considered, with only one drone and one truck. The truck moves on a predefined route and brings the drone close to the delivery point. Then, the drone plans its service route by choosing the take-off and landing points from which the delivery will be performed. We propose a constant time algorithm OSR to plan the drone route with minimum-energy service when the truck moves on a line in front of the deliveries (i.e., highway). Then, we devise the algorithm MS-OSR to plan a drone minimum-energy service route when the truck moves on a multiline that bounds a convex area where the deliveries take place. We found that OSR and MS-OSR plan drone service routes that save at least 30% and 60%, respectively, of the energy consumed by connecting the delivery and the truck following the shortest route, that is, following the perpendicular segment between the delivery point and the truck's route.**

***Index Terms*—Drone, Delivery Goods, Favorable winds, Energy, Trajectory Planning.**

I. Introduction

In recent years, drones or Unmanned Aerial Vehicles (UAVs) have been widely investigated in civil applications, such as agriculture, environmental protection, video monitoring, localization [1]–[4]. At the same time, delivery of packages has been announced by the Big company of e-commerce. Initially, it did not seem safe or practical to have tiny buzzing robots crisscrossing the sky. In the last two years, however, there are several reasons to believe that package delivery by drone may be coming soon, including the new regulations laws, just released in 2021 by the Federal Aviation Administration (FAA), that allow operators of small drones to fly over people and at night under certain conditions [5]–[7]. So it is highly expected that very soon transportation companies can further extend their business relying on drones that cross the last-mile to their customers. Deliveries with drones are potentially faster than with trucks because drones can connect points in the plane by traversing straight lines, without traffic or other impediments. However, delivery companies must be aware that the drone ranges must be short because the drones are battery-powered and the battery is limited in capacity due to the drone size. Also, strong winds can raise concerns during drone deliveries.

The work has been partially supported by "HALY-ID" project which has received funding from the European Union's Horizon 2020 under grant agreement ICT-AGRI-FOOD no. 862665, no. 862671, and from MIPAAF.

While the limitations due to strong gusts have been a primary concern so far for planning drone missions [6], to the best of our knowledge, not much attention has been given to the possibility of exploiting favorable wind conditions [8] to reduce the energy consumption of the drone. In this paper, we explore this possibility. Islands, like Corse, are very windy and favorable winds can be a great opportunity. Precisely, we propose to select the drone's trajectory for the last leg of the delivery route so that the wind is as favorable as possible. However, favorable wind over a too long route can make the energy saving for unit distance futile. So, the wind cannot be selected independently of the length of the traversed distance.

Due to the above considerations, our solution proposes to use a truck that brings the drone close to the delivery point. Then, pondered both the direction and the distance, we fly the drone along the trajectory that uses the least amount of energy for serving the delivery point. Using the drone, the truck avoids the detour from the main route up to the delivery point. Using the truck, the drone can operate in a short range. In a moderately dense ground environment, like a residential area neighborhood, already at a low altitude, the drone can freely move in the air having no obstacles on its way. Consequently, we assume that the drone serves the delivery point just following two straight lines from the take-off to the delivery point and from the delivery point to the landing point. Our goal is then to determine the take-off and landing points on the truck's route that minimize the battery consumption exploiting the most favorable wind conditions.

A. The related work

In the last five years, the problem of delivering goods with drones has been approached by several papers [9], [10]: an excellent and concise summary of the state of art is reported in [11]. Almost all the papers assume that the drone has unit-capacity and has to return to the warehouse after every single delivery due to the payload and energy budget constraints. Many solutions in the literature consider drones working in tandem with a mobile ground device (truck, van) and there are many ways the two means of transportation collaborate. Some solutions partition the deliveries between the two, some make them cooperate in every single mission [11]–[13] In our solution, truck and drone cooperate in every mission. From our point of view, the truck is an autonomous vehicle, not limited

in energy, moving on a predefined route, with no possibility to turn around and to detour from its route. It is at drone's disposal and brings the drone close to the delivery point. The drone completes the last leg of the delivery and is limited in energy budget. The truck and the drone aim to serve the end customer minimizing the energy spent by the drone. Although selecting the shortest trajectory between the truck's route and the delivery point could seem the winning strategy, this is not always the solution that minimize energy as we show in this paper. In a windy day, the drone can save energy if it serves the delivery point connecting the truck's route and the delivery point not with the oblique lines. Such oblique drone trajectory is also used in [12]–[14], but there the drone's route is given in input to the problem. In this paper, instead, the drone's trajectory is the output of our algorithm.

To the best of our knowledge, the impact of favorable winds on the planning of the drone trajectory has not received much attention so far. We believe that one of the reasons that have held back the researchers from studying such an impact is the difficulty of having simple and reasonable models that describe the drone energy consumption in terms of wind intensity and direction change. Recently, in [15], an energy model that permits to tabulate the expected energy consumed given the sort of drone used (quadcopter, octocopter), the speed of the drone, the payload, and the relative wind condition has been developed. From this model springs a line of research that considers wind conditions. In [16], the problem of finding which is the percentage of flight missions that can be successful accomplished with a given energy budget knowing the wind conditions on-the-fly was studied. The delivery problem has been modeled as finding the shortest path on a time-dependent weighted graph. The edge weights represent the energy spent to traverse the edges and the weights are time-dependent because the wind conditions vary during the time. However, in [16], the drone moves along predefined routes represented by the edges of the graph. In this work, instead, we exploit the freedom of selecting the drone trajectory that has the wind in favor to improve the energy efficiency. We found that, in presence of wind, often a longer distance is less energy demanding than the shortest one.

Contribution: Our results are summarized as follows:

1) We calculate the relative wind on any straight line that passes through the delivery point by building a coordinate system whose origin is the delivery point itself and the x-axis is parallel to the truck's route;
2) We propose a constant time algorithm (OSR) to plan the *optimal service route* when the truck moves on a line given the desired drone speed and the wind conditions;
3) We propose the algorithm *Multi-Side* OSR (MS-OSR), to plan a minimum-energy service route when the truck moves on a multi-line route that bounds the delivery area;
4) We simulate OSR and MS-OSR under two different set of winds: the exhaustive winds, which average the consumption on all the possible winds of the compass rose, and the real winds collected in few locations in Corse. We found that, OSR and MS-OSR save for each delivery, respectively, the 30% and 60% of energy with respect to the shortest drone's trajectory that connects the delivery point and the truck route. Recall that the shortest drone's trajectory coincides with the Euclidean distance between the delivery point and its projection on the truck's route.

Organization: The rest of the paper is organized as follows. Section II defines the relative winds and the compass rose, surveys the energy model, and computes the levels of energy associated with the winds of the compass rose. Section III proposes the OSR algorithm that determines the take-off and landing points of the drone on the truck's route that minimizes the energy spent to serve the end customer. Section IV extends OSR to the multi-line scenario. Then the performance of OSR and the MS-OSR extension are evaluated.

II. Model

In this section, we describe the main concepts we use to model the problem. First, we explain the wind system in Section II-A, then the energy model and the energy levels associated with the compass rose in Section II-B, and finally the truck-drone collaborative system in Section II-C.

A. The Wind

Wind is an important variable for drone energy consumption. The weather stations record the meteorologic wind which, during the day, can change speed and direction. The energy consumption increases if the drone movement and the wind are opposite, while decreases if the drone movement and the wind are equal. To evaluate the relative wind direction for the drone movement, we must convert the meteorological wind direction into the mathematical wind direction, as explained below.

a) Meteorologic and Mathematical Wind Directions: Weather stations record the *meteorologic direction* of the wind, that is, the direction from which the wind originates, assuming North as the 0 degree direction. For instance, if the wind blows from the north to the south, the weather station records a direction of 0 degrees, while if the wind blows from the east to the west, the weather station refers to 90 degrees. The meteorologic direction of the wind grows clockwise in a Cartesian coordinate system xOy whose x-axis is the North direction and the origin O is the destination (and not the source) of the wind. The *mathematical direction* of the wind, instead, considers the origin O as the source of the wind. The mathematical wind directions grow counterclockwise from the usual x-axis which is equal to the East direction. Hence, the conversion rule from the meteorological direction of the wind to the mathematical one is [17]:

$$w_d^{\mathrm{ma}} = |\underbrace{|-w_d^{\mathrm{me}}+360|_{360}}_{clockwise}\underbrace{+90}_{phase}\underbrace{-180}_{O}|_{360} = |-w_d^{\mathrm{me}}+270|_{360}$$

Fig. 1 shows the direction of the meteorological wind $w_d^{\mathrm{me}} = 225$ that is directed towards O and the corresponding mathematical direction $w_d^{\mathrm{ma}} = 45$ that has O as the source.

From now on, in our work, we only refer to the mathematical directions of the wind. All the directions of the wind

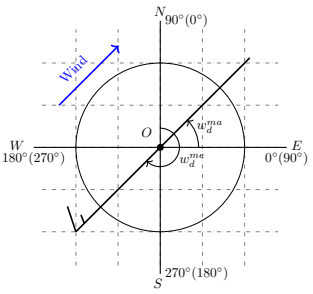

Fig. 1: The x and y axes are labelled with the cardinal, mathematical, and meteorologic (in brackets) directions.

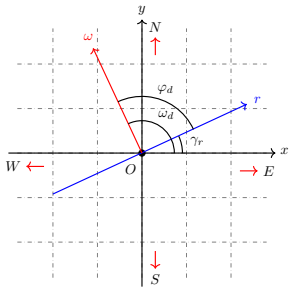

Fig. 2: Relative wind direction $\varphi(r) = 90°$ on the line r when $\gamma_r = 25°$ and $\omega_d = 115°$.

collected by the weather stations in Corsica in Section IV-B are converted in mathematical winds before applying the OSR and MS-OSR algorithms.

b) Global Wind and Relative Wind: The *global wind* ω is the wind that occurs in the area where the drone operates. The global wind $\omega = (\omega_d, \omega_s)$ is represented by the mathematical *direction* ω_d and its *speed* ω_s. The *relative wind* is the wind that the drone faces when it moves on a line r with direction γ_r under a global wind ω. The relative wind has *mathematical direction* $\varphi(\gamma_r, \omega)$ and speed φ_s. The relative direction $\varphi(\gamma_r, \omega) = |\omega_d - \gamma_r|_{360}$ is the difference mod 360 between the direction of the global wind and the direction of the drone movement (Fig. 2). In this paperwe assume $\varphi_s = \omega_s$, although in practice the flight altitude and the kind of the ground environment (i.e., urban, suburban, rural) can modify ω_s making $\varphi_s \geq \omega_s$. From now on, since in this paper we do not consider that the wind changes during a drone mission, while we consider different drone trajectories, we denote the relative direction $\varphi(\gamma_r, \omega)$ of the relative wind as $\varphi(r)$.

c) The Compass Rose: To define the *sector* winds and the *compass rose*, we divide the turn angle at O of a conventional Cartesian coordinate system xOy into $4t$ sectors, each of width $\sigma = 180/2t$ degrees. Conventionally, the *sector wind* S_i will contain the winds whose relative wind direction verifies

$$\left(i\frac{180}{2t}\ ;\ (i+1)\frac{180}{2t}\right] \quad 0 \leq i \leq 4t-1 \tag{1}$$

A *representative direction* ρ_i, with $0 \leq i \leq 4t-1$, will be associated to each sector wind S_i. The representative ρ_i will be used to compute the energy consumption of any relative wind direction that falls in S_i. In substance, the compass rose is used to limit to $4t$ the number of the possible energy levels, as we will see in the next section.

B. Energy Model and Levels of Energy

Recently in [15], a model to evaluate the energy $\mu(\upsilon_d, \omega_s, \varphi(r), \kappa)$ depleted to keep a drone travelling for 1 m, at a constant ground speed υ_d, along a trajectory r in direction γ_r, carrying a payload κ, and under a global wind ω was proposed. The energy is a function of the power Π required for producing the needed thrust to let the drone fly. Π depends on the drone's rotor characteristics, and on the square of the drone's relative air speed $\upsilon_a(r) = |\sqrt{\upsilon_d^2 + \omega_s^2 - 2\upsilon_d\omega_s\cos(\varphi(r))}|$. As reported in [16], [18], since Π is calculated by solving an implicit equation, we cannot give a close formula for the power and for the energy as well. However, the energy can be tabulated for different drone and wind speeds, different payloads, and for the $4t$ different relative winds of the compass rose.

TABLE I: Energy coefficients μ_i with different payloads κ and $\upsilon_d = 10\,\mathrm{m/s}$, $\omega_s = 10\,\mathrm{m/s}$.

μ_i	Payload κ (Kg)		
S_i	0	2	6
0	0.1235395549	0.1511641188	0.2126169706
1	0.1487165204	0.1770355558	0.2398070629
2	0.2216461515	0.2511850333	0.316473693
3	0.4462761438	0.4787047231	0.5491670144
4	0.534990835	0.5692753882	0.6425861937
5	0.5677098232	0.6027887907	0.6773260158
6	0.5676725759	0.6027506094	0.6772863865
7	0.5328310777	0.567065102	0.640298223
8	0.4426247141	0.4749871414	0.5453470678
9	0.2184914376	0.2479916775	0.3131969116
10	0.1471049048	0.1753853793	0.2380818085
11	0.1235135924	0.1511373263	0.21258864

In our paper, we will use energy values tabulated under different conditions. When υ_d, ω_s, and κ are clear from the context, we simply denote the energy spent under the sector wind S_i as μ_i, with $0 \leq i \leq 4t-1$. Table I reports the 12 different energy levels of a compass rose with $t = 3$, and thus $\sigma = 30°$. For computing the energy consumption, we select as ρ_i the angle in S_i whose cosine is maximum in absolute value (e.g., $\rho_0 = 1°$ in S_0 and $\rho_{11} = 0°$ in S_{11}. With this representative, μ_0 and μ_{11} are almost the same). When the cosine of the representative wind is negative (see for example S_3 with respect S_2), μ_i increases because $\upsilon_a(r)$ increases. Table I also reports the different energy levels below different payloads.

Finally, the energy spent by a drone to traverse a given distance δ facing the sector wind S_i is given by the product of $\mu_i\delta$, with $0 \leq i \leq 4t-1$.

C. The OSR problem

In this paper, the drone D is carried by a truck, named MT. When a delivery point P that has to be served by the drone approaches, the drone selects on the truck path the take-off and landing points, called X_T and X_L, respectively. The drone flies on the straight line from X_T to P carrying the payload. After dropping off the payload, the drone empty moves back on the straight line from P to X_L, as illustrated in Fig. 3. The drone and the truck always move forward in the sense that the projection H of P onto the MT path must follow X_T and precede X_L. As said, the MT never turns back to pick up the drone. Changing X_T and X_L, the slope of the segments X_TP and PX_L changes and the relative winds $\varphi(X_TP)$ and $\varphi(PX_L)$ change too. Also, the lengths of $\overline{X_TP}$ and $\overline{PX_L}$

change. In this paper, we want to find the *optimal service route* $X_T P X_L$, that is, the last mile trajectory that minimizes the energy consumed by the drone to serve P.

III. The Optimal Service Route Algorithm

In this section, we assume to have in input the MT's route represented by a straight line r and the truck's movement direction γ_r, a delivery point P, and a global wind ω. Our goal is to find the *optimal service route* OSR that minimizes the energy spent by the drone to fly towards P and return back on the MT's path. OSR is uniquely identified by the take-off point T and the landing point L on r.

We reason as follows. On r there are many points from which the drone can take off and land. Fixed the global wind in the area, the drone faces a relative wind denoted as $\varphi(\overrightarrow{X_T P})$ and $\varphi(\overrightarrow{P X_L})$, respectively, for each take-off or landing trajectory. In principle, there are infinite relative winds (one for each take-off X_T or landing X_L point on r), but since we have grouped the relative wind directions, there are at most $4t$ sector winds to be considered. Each sector wind requires a different energy level. Among all the X_T's or X_L's points that fall into the same sector wind and thus require the same energy for unit distance, the one that consumes less energy is the closest to P. Among the $4t$ different shortest take-off and landing trajectories associate to the $4t$ sector winds, OSR selects the take-off and landing trajectories that consume the minimum energy to serve P. In the rest of this section, we implement this reasoning. We first show how to compute the relative wind directions on the possible D's routes, then we determine the sector winds corresponding to them, and then we find the best route for each sector wind. Finally, we summarize the procedure to compute OSR in Alg. 1.

A. Relative Wind Determination

From now on, let $r = mx + q$ be the MT's route. Consider the Cartesian coordinate system xPy of the mathematical wind, with origin in P. We distinguish two cases [1]:

1) P is on the left of MT when it moves along r, or
2) P is on the right of MT when it moves along r.

Let H be the projection of P on r. We assume that any *candidate take-off point* $X_T \in r$ is on the left of H, i.e., $X_T \leq H$. Similarly, any *candidate landing point* X_L is on the right of H, i.e., $X_L \geq H$.

Theorem 1. *The relative winds on* $\overrightarrow{X_T P}$ *and* $\overrightarrow{P X_L}$ *are:*

$$\varphi(\overrightarrow{X_T P}) = \begin{cases} |\omega_d - (\gamma_r + \alpha(HX_T P))|_{360} & \text{if } P \text{ on the left of } r \\ |\omega_d - (\gamma_r - \alpha(HX_T P))|_{360} & \text{if } P \text{ on the right of } r \end{cases}$$

$$\varphi(\overrightarrow{P X_L}) = \begin{cases} |\omega_d - (\gamma_r - \alpha(PX_L H))|_{360} & \text{if } P \text{ on the left of } r \\ |\omega_d - (\gamma_r + \alpha(PX_L H))|_{360} & \text{if } P \text{ on the right of } r \end{cases} \quad (2)$$

Proof. We prove (2) when P is on the left of r (see Figure 3a). Consider the rotate Cartesian system $x_r P y_r$ with origin in P, x_r-axis parallel to r and oriented in the same direction as r. Recall that the y_r-axis forms a 90° counter-clockwise angle with x_r. Note that the angle between x and x_r has width γ_r. In

[1]The position of P with respect to r can be easily checked in constant time by testing if r moves counterclockwise or clockwise to reach P.

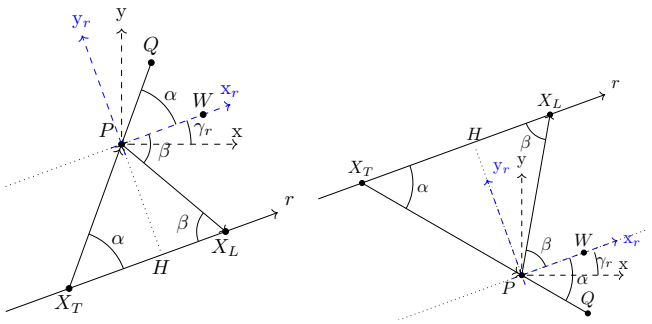

(a) P is on the left of r. (b) P is on the right of r.

Fig. 3: The relative winds on $X_T P$ and $P X_L$.

Figure 3a, for clarity, we denote $\alpha(HX_T P)$ simply as α and $\alpha(PX_L H)$ as β. Fixed the position of X_T, we can calculate $\alpha = \arctan \frac{\overline{PH}}{\overline{X_T H}}$. Observed that r and x_r are parallel, $\overrightarrow{X_T P}$ forms the same angle $\alpha = \widehat{WPQ}$ on $x_r P y_r$ and the angle $(\gamma_r + \alpha)$ on xPy. Hence, the direction of the relative wind on xPy is $\varphi(\overrightarrow{X_T P}) = \omega_d - (\gamma_r + \alpha(HX_T P))$.

Fixed the position X_L on r, it holds $\beta = \arctan \frac{\overline{PH}}{\overline{HX_L}}$. Observed that r and x_r are parallel, the returning path $\overrightarrow{PX_L}$ forms the angle $-\beta$ on $x_r P y_r$. Hence, the direction of the relative wind on xPy is $\varphi(\overrightarrow{PX_L}) = \omega_d - (\gamma_r - \beta) = \omega_d - (\gamma_r - \alpha(PX_L H))$.

The case where P is on the right of r is depicted in Figure 3b. Eq. 2 can be proved similarly to the left case. □

B. Grouping Relative Winds

We study in which sector wind the relative winds of the D's trajectories fall. First, observe that the relative wind on the MT's route is $\varphi(r) = |\omega_d - \gamma_r|_{360}$, and, fixed the compass rose cardinality t, let S_τ where $\tau = \left\lfloor \frac{|\varphi(r)-1|_{360}}{\sigma} \right\rfloor$ be the relative sector wind on the MT's route. Note that τ depends on $\varphi(r)-1$ instead of $\varphi(r)$ because the sectors in (1) are defined open on the left extreme and close on the right extreme.

Denote the angle formed by the D's route with the MT's route as $\widehat{D}$ and its width as $\alpha(D)$. When X_T and X_L move on r until H (see Fig. 3), it is easy to see that $\alpha(D)$ vary in the interval $(0, 90]$. Precisely, $\alpha(HX_T P) = \alpha(PX_L H) = 90$ when $X_T H = HX_L = 0$, while $\alpha(HX_T P) = \alpha(PX_L H) = 0$ when $X_T H = HX_L \to \infty$. Then, the relative winds on the take-off and landing D's trajectories, scan the first quadrant (I Q) or the fourth quadrant (IV Q) of the Cartesian coordinate system with origin in P and whose x-axis coincides with the relative wind $\varphi(r)$ (illustrated in blue in Fig. 4). From that, (2) can be rewritten as:

$$\varphi(\overrightarrow{X_T P}) = \begin{cases} |\varphi(r) - \alpha(HX_T P))|_{360} & \text{if } P \text{ on the left of } r \quad IVQ \\ |\varphi(r) + \alpha(HX_T P))|_{360} & \text{if } P \text{ on the right of } r \quad IQ \end{cases}$$

$$\varphi(\overrightarrow{P X_L}) = \begin{cases} |\varphi(r) + \alpha(PX_L H))|_{360} & \text{if } P \text{ on the left of } r \quad IQ \\ |\varphi(r) - \alpha(PX_L H))|_{360} & \text{if } P \text{ on the right of } r \quad IVQ \end{cases} \quad (3)$$

By (3) and (1), it holds:

Algorithm 1: OSR

INPUT: r - MT's route; ω - global wind; P - delivery point;
t - cardinality of sector winds;
$\mu_0^\kappa, \mu_1^\kappa, \ldots, \mu_{4t-1}^\kappa$ - precomputed energy levels with payload;
$\mu_0, \mu_1, \ldots, \mu_{4t-1}$ - precomputed energy levels without payload
OUTPUT: T and L on r, along with the energy $E(TP)$ and $E(PL)$
begin;
$\varphi(r) = |\omega_d - \gamma_r|_{360}$;
$\tau = \left\lfloor \frac{|\varphi(r)-1|_{360}}{\sigma} \right\rfloor$;
$\overline{HP}$ is the distance of P from r;
if *P is on the left of r* **then**
    ▷ Find T and $E(TP)$;
    $\varphi(X_T P)$ scans the IV Q ; ▷ see Eq. 3
    Let $j^* = \arg\{\min_{0\le j\le t}\{\frac{\mu^\kappa_{|\tau-j|_{4t}}}{\sin(\Lambda(|\tau-j|_{4t}))}\}\}$; ▷ Tab. II
    Set T : $\overline{TH} = \overline{PH}\cot(\Lambda(|\tau - j^*|_{4t})$;
    $E(TP) = \left(\mu^\kappa_{|\tau-j^*|_{4t}}\right) \frac{\overline{PH}}{\sin(\Lambda(|\tau-j^*|_{4t}))}$;
    ▷ Find L and $E(PL)$;
    $\varphi(PX_L)$ scans the I Q ; ▷ see Eq. 3
    Let $j^* = \arg\{\min_{0\le j\le t}\{\frac{\mu_{|\tau+j|_{4t}}}{\sin(\Lambda(|\tau+j|_{4t}))}\}\}$; ▷ Tab. II
    Set L : $\overline{HL} = \overline{HP}\cot(\Lambda(|\tau + j^*|_{4t})$
    $E(PL) = \left(\mu_{|\tau-j^*|_{4t}}\right) \frac{\overline{PH}}{\sin(\Lambda(|\tau-j^*|_{4t}))}$;
if *P is on the right of r* **then**
    ▷ Find T and $E(TP)$;
    $\varphi(X_T P)$ scans the I Q ; ▷ see Eq. 3
    Let $j^* = \arg\{\min_{0\le j\le t}\{\frac{\mu^\kappa_{|\tau+j|_{4t}}}{\sin(\Lambda(|\tau+j|_{4t}))}\}\}$; ▷ Tab. II
    Set T : $\overline{TH} = \overline{PH}\cot(\Lambda(|\tau + j^*|_{4t})$;
    $E(TP) = \left(\mu^\kappa_{|\tau+j^*|_{4t}}\right) \frac{\overline{PH}}{\sin(\Lambda(|\tau+j^*|_{4t}))}$;
    ▷ Find L and $E(PL)$;
    $\varphi(PX_L)$ scans the IV Q ; ▷ see Eq. 3
    Let $j^* = \arg\{\min_{0\le j\le t}\{\frac{\mu_{|\tau-j|_{4t}}}{\sin((\Lambda(|\tau-j|_{4t}))}\}\}$; ▷ Tab. II
    Set L : $\overline{HL} = \overline{PH}\cot(\Lambda(|\tau - j^*|_{4t})$;
    $E(PL) = (\mu_{|\tau-j^*|_{4t}}) \frac{\overline{PH}}{\sin(\Lambda(|\tau-j^*|_{4t}))}$;
    end
return T *and* L

Theorem 2. *When $\varphi(\overrightarrow{X_T P})$ or $\varphi(\overrightarrow{PX_L})$ scan the first quadrant (I Q in (3)), the drone faces the winds S_i of the compass rose whose indices i are:*

$$\tau \le i \le |\tau + t|_{4t} \tag{4}$$

When $\varphi(\overrightarrow{X_T P})$ or $\varphi(\overrightarrow{PX_L})$ scan the fourth quadrant (IV Q in (3)), the indices of the scanned winds S_i are :

$$|\tau - t|_{4t} \le i \le \tau \tag{5}$$

As an example, in Fig. 4, the sector winds scanned by the D's trajectories with $t = 3$, $\sigma = 30°$ and $\varphi(r) = 50°$ are S_1, S_2, S_3, and S_4 in the first quadrant, and S_1, S_0, S_{11}, and S_{10} in the fourth quadrant.

To complete our analysis, it remains to find for each sector wind scanned by the D's routes, the shortest take-off and landing paths.

Since the length of the D's route is $\frac{\overline{PH}}{|\sin(\alpha(D))|}$ and since $\alpha(D) \in (0, 90]$, the shortest take-off and landing D's routes in each S_i correspond to the largest values $\alpha(D)$.

For the $t+1$ sector winds scanned by the D's trajectories, Table II lists the smallest $\xi(i)$ and the largest $\Lambda(i)$ values that fall in S_i. $\Lambda(i)$ gives the shortest route in S_i. The sector wind S_{i^*} that requires the minimum energy to reach P, that is $i^* = \arg\min\{\frac{\mu_i}{\sin(\Lambda(i))}\}$, is the most favorable sector wind to be selected. Namely, the energy in S_i to reach P is given by the distance $\frac{PH}{\sin(\Lambda(i))}$ multiplied by μ_i.

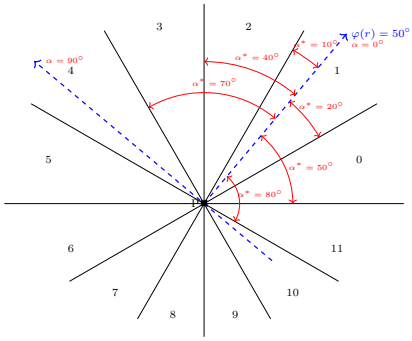

Fig. 4: The winds of the compass rose scanned by the different drone trajectories $X_T P$ and PX_L when $\varphi(r) = 50°$.

TABLE II: The angles $\alpha(D) \in (0, 90]°$ associated to each wind $S_{|\tau+j|_{4t}}$ of the I and IV quadrant of $\varphi(r)$

I Quadrant			
$\alpha(D)$			
Smallest $\xi(|\tau + j|_{4t})$	**Largest** $\Lambda(|\tau + j|_{4t})$	**Wind**	j
1	$(\sigma - |\varphi(r)|_\sigma)$	S_τ	0
$-|\varphi(r)|_\sigma + j\sigma + 1$	$-|\varphi(r)|_\sigma + (j+1)\sigma$	$S_{|\tau+j|_{4t}}$	$1 \le j \le t-1$
$-|\varphi(r)|_\sigma + t\sigma + 1$	90	$S_{|\tau+t|_{4t}}$	t

IV Quadrant			
$\alpha(D)$			
Smallest $\xi(|\tau - j|_{4t})$	**Largest** $\Lambda(|\tau - j|_{4t})$	**Wind**	j
1	$|\varphi(r)|_\sigma - 1$	S_τ	0
$|\varphi(r)|_\sigma + j\sigma$	$|\varphi(r)|_\sigma + (j+1)\sigma - 1$	$S_{|\tau-j|_{4t}}$	$1 \le j \le t-1$
$|\varphi(r)|_\sigma + t\sigma$	90	$S_{|\tau-t|_{4t}}$	t

Last, note that, since the drone flies towards P loaded and returns unloaded towards the MT, two different levels of energy, one including the payload μ_i^κ and one without payload μ_i, are used to compute the overall drone's energy consumed to complete the mission.

Table III reports the sector winds and the range of values of $\alpha(D) \in (0, 90]°$ associated to each sector wind of the I and IV quadrant when $\varphi(r) = 50°$, $\tau = 1$, and $t = 3$, as in the Example in Fig. 4. Our discussion to find OSR is recap in Alg. 1. In conclusion:

Fact 1. *Given the* MT *route r and γ_r, the delivery point P, the wind ω, the drone speed v_d, and fixed t of the compass rose,* OSR *computes in $O(1)$ time the two straight line TP and PL that consume the minimum energy to serve P from r.*

TABLE III: The angles $\alpha(D) \in (0, 90]°$

I Quadrant				IV Quadrant			
$\alpha(D)$		**Wind**	j	$\alpha(D)$		**Wind**	j
1	10	S_1	0	0	19	S_1	0
11	40	S_2	1	20	49	S_0	1
41	70	S_3	2	50	79	S_{11}	2
71	90	S_4	3	80	90	S_{10}	3

IV. Multi-line extension and Simulations

We evaluate the impact of selecting the optimal service route OSR on energy consumption. We study the energy cost when the drone operates from a single-line (case study *line*) and it can select from which line to operate among multiple lines (case study *multi-line*). In the first case, the MT travels on a straight line (i.e., highway) and the deliveries occur in the area in front of the highway, in the second case the MT circumnavigates the area where the deliveries occur.

We consider two types of winds in the experiments: *exhaustive winds* EW and *real winds* RW. In EW, we vary ω_d with regular steps between 1° and 360° and consequently the relative wind $\varphi(r)$ on r varies. In RW, the wind varies according to the data collected at different hours of the day in two locations in Corsica during winter days: the wind of Corte (inland) is characterized by low wind speed, while those of Cap Corse (seaside) have high wind speed.

Section IV-A describes the generation of our tests, while Section IV-B presents the results.

A. Description

1) Line: We consider the MT's route $r: \ y = 0$ with $\gamma_r = 0$ and a single fixed point P to be served at distance $6\,\mathrm{Km}$ from r. To serve P we compare two algorithms:

- Optimal trajectory (OSR): Alg. 1 is applied to r and P to find the take-off T and landing L points.
- Shortest trajectory (E) : P is served selecting the shortest route HP from r to P, that is, the take-off and the landing points coincide with H.

2) Multiline: In this scenario, we consider a delivery area, which consists of a circle of radius $R = 5\,\mathrm{km}$. Inside, the circle we generate a convex polygon with $n = 8$ sides. Setting the starting point of the MT's route as one of the vertices of the polygon, the route follows by the sequence of vertices $\{s_0, s_1, ..., s_7\}$ traveled in a clockwise direction. An example is illustrated in Fig. 5. Even if the wind does not change, the relative winds on the lines change, and so the optimal service route may differ from line to line. We consider a set of 20 delivery points randomly generated inside the polygon. For each delivery, the optimal service route is obtained by applying Algorithm OSR from each polygon side. Four different algorithms are proposed:

- Same Side Optimal trajectory (SS-OSR): This approach applies Alg. 1 to each side of the polygon and returns the pair T and L on the side that consumes the minimum energy. Both T and L are forced to belong to the same line. To be precise, we apply OSR only to those sides that contain the projection H of P. Since each polygon's side has a limited size, not all the values in $(0, 90]$ can be taken by $\alpha(D)$. SS-OSR is applied to serve P_0 in Fig. 5.
- Multiple Optimal trajectory (MS-OSR) : It is similar to SS-OSR, but T and L are not forced to belong to the same side. The computations of TP and PL in OSR are uncoupled. First, OSR is applied to each side of the polygon to find the minimum energy take-off trajectory TP, and then OSR is applied to each side of the polygon to find the minimum energy landing trajectory LP. The constraint that the MT cannot go back is respected selecting T that (clockwise) precedes L on the MT route. As an example, MS-OSR is applied to find T and L to serve P_1 in Fig. 5.
- Same Side Shortest distance (SS-E): it is like SS-OSR but it invokes for each side, algorithm E instead of OSR. For each side, it is considered the trajectory that serves P by the projection H of P on that side. Then, P will be served starting from the side that minimizes the energy consumption. Recall that this is not necessarily the side closer to P because the energy spent depends also on the relative wind on the take-off and landing trajectory. SS-E is applied to serve P_2 in Fig. 5.
- Multiple Shortest trajectory (MS-E): it is like MS-OSR but it applies E instead of OSR. This solution serves P using only the shortest Euclidean routes, as SS-E. However, it allows that the take-off and landing point lie on different sides, as MS-OSR. MS-E is applied to serve P_3 in Fig. 5.

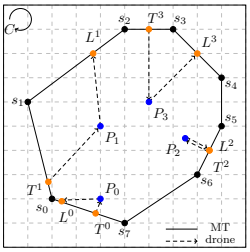

Fig. 5: Illustration of the possible D trajectories.

B. Evaluation

We evaluate our solution computing the energy and the distance to serve a single delivery point using the above algorithms. We evaluate the distance to show that running in a favorable wind, D can save energy even if the traveled distance is longer than the Euclidean distance between the MT's route and the delivery point P.

In the line scenario, P is fixed. We repeat the mission under different winds. For each mission, we compute the energy and distance costs and we average the costs over all the evaluated different winds. In the multi-line scenario, for each mission, we fix a global wind w and we serve all the 20 points. We compute the average delivery energy for each mission as the total depleted energy divided by 20. Then, we repeat the mission under different winds and again we average the delivery energy over all the missions.

1) Line: Fig. 6 compares the average energy and distances depleted by Algorithms OSR and E in a single line scenario. With Algorithm E, the drone always travels the same distance $12\,\mathrm{Km}$ as P is at $6\,\mathrm{Km}$ from r. For each mission, we compute the energy consumed by OSR and E. Note that E does not spend the same amount of energy going to P and coming back not only because going the drone carries a payload while coming back the drone is empty, but also because the sector

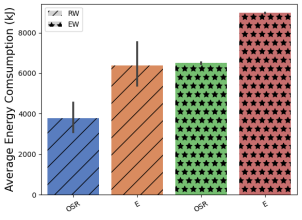

(a) Average energy.

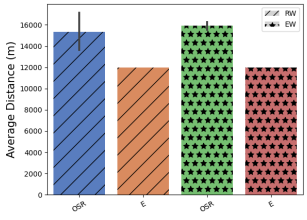

(b) Average distance.

Fig. 6: The performance of OPT and E in the line scenario with $v_d = 20\,\mathrm{m/s}$ and $\kappa = 6$.

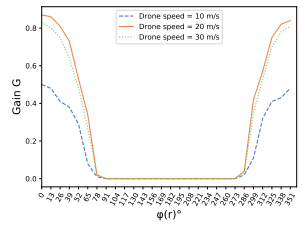

(a) $\gamma_r = 0°$

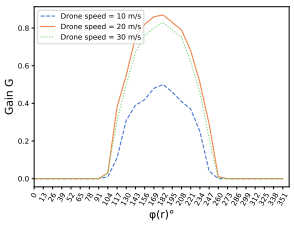

(b) $\gamma_r = 180°$

Fig. 7: Tests EW with $\omega_s = 20\,\mathrm{m/s}$ and $\kappa = 6\,\mathrm{kg}$.

wind may be different due to the different verses. The plots report the average energy consumption when $v_d = 20\,\mathrm{m/s}$, $\gamma_r = 0$, $\kappa = 6$, and $t = 3$. The results labelled EW are obtained by fixing $\omega_s = 20\,\mathrm{m/s}$ and by varying ω_d among all the multiples of $13°$ and $30°$ in $(0, 360]$. Instead, the results labeled RW are obtained by varying ω, both speed and direction, on a set of winds collected in Corse in 10 days.

The results in Fig. 6 are very interesting: under RW, for each mission, OSR saves forty percent of the energy of E although it crosses one-fourth longer distances than E. Under EW, OSR saves thirty percent of the energy with respect to E and travels one-third more than E. These results show that our investigation of the impact of the wind on flight energy is worthy. The EW and RW saving are quite similar, although EW saves more than RW because EW spans all the possible winds and half of them are favorable winds, while RW follows the weather and not all the winds have the same probability to occur. Consequently, EW is more stable than RW experiments as shown by the confidence intervals.

The EW tests scan all the possible winds. Thus, we plot the *energy gain* G which is defined as the ratio between the energy saved by Algorithm OSR with respect to E, over the energy spent by E. Fig. 7 plots the gain when ω_d is a multiple of $13°$ in $(0, 360]$. By definition,G does not depend on the distance PH but only on the energy spent per unit of distance.

Inspecting Fig. 7a, OSR gains with respect to E in half of the exhaustive winds. G is superior to 0 when $\varphi(r) = |\omega_d - \gamma_r|_{360} = \omega_d \in (0, 90] \cup (270, 360]$ and it can reach up to the 80% under relative winds. G decreases when ω_d approaches $90°$ or $270°$. In all the other cases, $90 < \omega_d \leq 270$, OSR and E

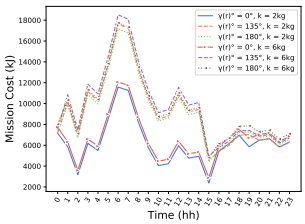

(a) Different payloads

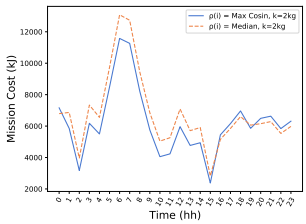

(b) Different representative $\rho(i)$.

Fig. 8: Test RW with $v_d = 20\,\mathrm{m/s}$ and $t = 3$.

coincide and $G = 0$, that is, the shortest path is the best route. We conclude that the savings are higher in the line scenario the more $\varphi(r)$ falls in $(0, 90] \cup (270, 360]$.

Note that changing γ_r, the curve of the gain just rotates. For example, when $\gamma_r = 180°$ in Fig. 7b, OSR will beat E when ω_d falls in $(180, 270] \cup (90, 180]$, while OSR and E coincide when ω_d in $(0, 90] \cup (270, 360]$.

In Fig. 7, we also evaluate the impact of different drone speeds on the gain. Observe that the gain is maximum when $\omega_s = v_d$, which is the case when the thrust Π that has to be provided to let the drone fly is the minimum one. It is worthy to note that the gain decreases more when the drone has to be slowed down ($v_d = 10\,\mathrm{m/s}$) than when the drone must accelerate ($v_d = 30\,\mathrm{m/s}$) with respect to the wind speed. So a stronger thrust is required to decelerate than to accelerate.

Finally, Fig. 8 reports the energy spent under different payloads and different representatives. To evaluate the impact of these parameters we select the real winds of a typical day of the seaside in Corse. As one can see, the impact is moderated in both cases. In particular, the increase on the depleted energy with different payloads is almost independent of the line direction γ_r and coherent with the values tabulated in Table I. The mission energy cost, when the representative $\rho(i)$ is the median angle in S_i, is slightly larger than the energy cost when $\rho(i)$ is the angle in S_i whose cosine is maximum in absolute value. However, a deeper investigation of real data is required to decide which is the best representative.

2) Multiline: Here, the drone has the freedom to decide from which side of the polygon to serve the delivery point.

Fig. 9 shows the energy consumed and the distance traversed to serve a single mission under EW and RW. Precisely, the four algorithms SS-OSR, MS-OSR, SS-E, and MS-E are examined.

MS-OSR is the most energy-efficient algorithm in both wind scenarios, although it travels on average the longest distance. Under the EW winds, MS-OSR more than halves the energy of SS-OSR for a single delivery by the freedom of selecting T and L on two different sides. The same happens for SS-E and MS-E. As seen for the single line, SS-OSR saves about 40% of the energy of SS-E and MS-OSR consumes one-third of the energy of SS-E, thus saving at least 60%. MS-OSR saves 20% of energy with respect MS-E. It is worthy to note the good performance of MS-E with respect to SS-OSR: although SS-OSR depletes less energy than MS-E, (precisely, SS-OSR

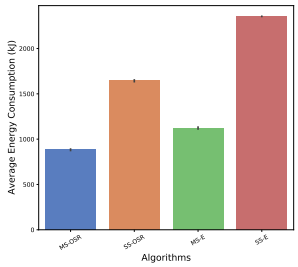

(a) Average energy with EW.

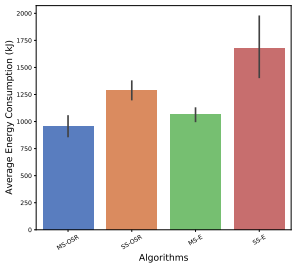

(b) Average energy with RW.

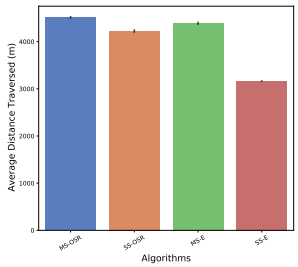

(c) Average distances with EW.

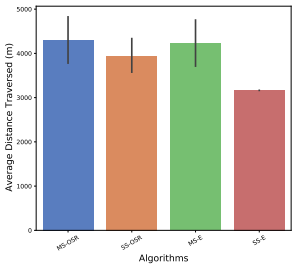

(d) Average distances with RW.

Fig. 9: Multi-line tests with $v_d = 20\,\mathrm{m/s}$, $\kappa = 6\,\mathrm{kg}$, and $t = 3$.

consumes 20% less than MS-E), one cannot forget to read the MS-E performance in light of its simplicity: MS-E that just selects its trajectories among the shortest paths. Regarding the traveled distances, algorithms that save more energy travel more. Note that, since the polygon is inscribed in a circle of radius $R = 5\,\mathrm{Km}$, each delivery point is at most at distance $10\,\mathrm{Km}$ from the polygon's side, but all the algorithms serve the delivery traversing on average a distance between $3\,\mathrm{Km}$ and $4.5\,\mathrm{Km}$. Under the RW winds, the algorithms follow exactly the same behavior as under EW. However, as seen for the single line scenario, the algorithms save slightly less energy, the traversed distance is shorter, and the results are more variable as evidenced by the wider confidence interval.

In conclusion, being able to choose between several sides of the polygon we save a lot. In fact, not only do we choose the side with the most favorable wind, but also the distance decreases significantly: a couple of deliveries can be fulfilled easily with regular batteries of $5\,\mathrm{kJ}$ in use in nowadays COTS drone against the single delivery achievable in the line scenario.

V. Conclusions

For the first time, at the best of our knowledge, we include the wind in the drone routing problem. We investigate the problem of finding the best route for a delivery drone that takes off from a truck and must deliver some goods to a know destination. Two algorithmic solution are proposed: for when the truck moves on a line (as on a highway) in front of the deliveries, and for when the truck moves on a multi-line that bounds a convex area where the deliveries take place.

In the future, we would like to confirm our findings by using flight simulators, and then by extending our investigation to a test-bed made of COTS drones. We also will include discussions on what can go wrong, e.g. time of day/night when the winds may be unstable, and on how to include the flight time scheduling because there are different winds at different hours of the day.

Acknowledgment

The authors are grateful to Patric Botey, director of R&D Projets Europeens Civil Protection at SDIS, and to Florence Vayess, Referente Nationale of Meteo-France for providing real data.

References

[1] H. Shakhatreh, A. H. Sawalmeh, A. Al-Fuqaha, Z. Dou, E. Almaita, I. Khalil, N. S. Othman, A. Khreishah, and M. G., "Unmanned aerial vehicles (uavs): A survey on civil applications and key research challenges," *IEEE Access*, vol. 7, pp. 48 572–48 634, 2019.

[2] F. Betti Sorbelli, C. M. Pinotti, and G. Rigoni, "Range-free localization algorithms with mobile anchors at different altitudes: A comparative study," in *Proceedings of the 21st International Conference on Distributed Computing and Networking*, 2020, pp. 1–10.

[3] F. Betti Sorbelli, S. K. Das, C. M. Pinotti, and G. Rigoni, "A comprehensive investigation on range-free localization algorithms with mobile anchors at different altitudes," *Pervasive and Mobile Computing*, vol. 73, p. 101383, 2021.

[4] A. Trotta, F. D. Andreagiovanni, M. Di Felice, E. Natalizio, and K. R. Chowdhury, "When uavs ride a bus: Towards energy-efficient city-scale video surveillance," in *IEEE INFOCOM 2018 - IEEE Conference on Computer Communications*, 2018, pp. 1043–1051.

[5] D. Schneider, "The delivery drones are coming," *IEEE Spectrum*, vol. 57, no. 1, pp. 28–29, 2020.

[6] "On demand drone delivery," https://flytrex.com/, 2020, [Online; accessed 12-01-2021].

[7] "Research-driven solutions to critical challenges in the uas industry," https://vtnews.vt.edu/articles/2020/11/ictas-maap-UPP2.html, 2020, [Online; accessed 07-01-2021].

[8] C. C. Murray and A. G. Chu, "The flying sidekick traveling salesman problem: Optimization of drone-assisted parcel delivery," *Transportation: Emerging Technologies*, vol. 54, pp. 86–109, 2015.

[9] A. Otto, N. Agatz, J. Campbell, B. Golden, and E. Pesch, "Optimization approaches for civil applications of unmanned aerial vehicles (uavs) or aerial drones: A survey," *Networks*, vol. 72, no. 4, pp. 411–458, 2018.

[10] N. A. Agatz, P. Bouman, and M. Schmidt, "Optimization approaches for the traveling salesman problem with drone," *ERIM Report Series Reference No. ERS-2015-011-LIS*, 2018.

[11] J. C. de Freitas and P. H. V. Penna, "A variable neighborhood search for flying sidekick traveling salesman problem," *International Transactions in Operational Research*, vol. 27, no. 1, pp. 267–290, 2020.

[12] G. C. Crişan and E. Nechita, "On a cooperative truck-and-drone delivery system," *Procedia Computer Science*, vol. 159, pp. 38–47, 2019.

[13] N. Boysen, D. Briskorn, S. Fedtke, and S. Schwerdfeger, "Drone delivery from trucks: Drone scheduling for given truck routes," *Networks*, vol. 72, no. 4, pp. 506–527, 2018.

[14] R. Roberti and M. Ruthmair, "Exact methods for the traveling salesman problem with drone," *Transportation Science*, 2021.

[15] J. K. Stolaroff, C. Samaras, E. R. O'Neill, A. Lubers, A. S. Mitchell, and D. Ceperley, "Energy use and life cycle greenhouse gas emissions of drones for commercial package delivery," *Nature communications*, vol. 9, no. 1, pp. 1–13, 2018.

[16] F. Betti Sorbelli, F. Corò, S. K. Das, and C. M. Pinotti, "Energy-Constrained Delivery of Goods With Drones Under Varying Wind Conditions," *IEEE Transactions on Intelligent Transportation Systems*, pp. 1–13, 2020.

[17] J. M. Wallace and P. V. Hobbs, *Atmospheric science: An introductory survey*. Amsterdam: Elsevier Academic Press., 2006.

[18] W. Johnson, *Helicopter theory*. Courier Corporation, 2012.